

## Article

# Treatment of Acidic Solutions Containing As(III) and As(V) by Sulfide Precipitation: Comparison of Precipitates and Sulfurization Process

Hui Xu <sup>1</sup>, Yunyan Wang <sup>1,2,3,\*</sup>, Liwei Yao <sup>4,\*</sup>, Yong Ke <sup>1,2,3</sup>, Yongjian Luo <sup>1</sup>, Limin Zhang <sup>1</sup>, Jiali Du <sup>1</sup>, Lin Yu <sup>1</sup>, Junjie Cao <sup>1</sup> and Xiaobo Min <sup>1,2,3</sup>

<sup>1</sup> School of Metallurgy and Environment, Central South University, Changsha 410083, China

<sup>2</sup> Chinese National Engineering Research Center for Control & Treatment of Heavy Metal Pollution, Changsha 410083, China

<sup>3</sup> Water Pollution Control Technology Key Laboratory of Hunan Province, Changsha 410004, China

<sup>4</sup> College of Resources and Environment, Hunan Agricultural University, Changsha 410128, China

\* Correspondence: wyy@csu.edu.cn (Y.W.); yaoliwei0125@126.com (L.Y.)

**Abstract:** Sulfide precipitation has been widely applied to remove arsenic from acidic wastewater containing As(III) and As(V), due to its simple process and high efficiency. However, the characteristics and composition of the precipitates are also of importance for its further treatment and disposal. To explore the characteristics of elemental S formed by reduction and the combined form of the generated S and As<sub>2</sub>S<sub>3</sub>, the characteristics of precipitates sulfurized from As(III) and As(V) and the effects of temperature, the S(-II) to As ratio (S/As), Cl<sup>-</sup> concentration (c<sub>Cl<sup>-</sup></sub>), and the volume fraction of H<sub>2</sub>SO<sub>4</sub> (φ<sub>H<sub>2</sub>SO<sub>4</sub>(v)</sub>) on the sulfurization of As(III) and As(V) were investigated in detail. The results showed that the contents of As and S were 60.37% and 39.73% in precipitate-As(III), while they accounted for 47.46% and 52.64% in precipitate-As(V); both precipitate-As(III) and precipitate-As(V) were mainly composed of amorphous As<sub>2</sub>S<sub>3</sub>, while the latter contained elemental S. Temperature and S(-II)/As(III) slightly affected the sulfurization process of As(III), while for As(V), as the temperature increased, the content of As<sub>2</sub>S<sub>3</sub> in precipitate-As(V) increased significantly. Additionally, with the S(-II)/As(V) increasing, the content of As<sub>2</sub>S<sub>3</sub> increased continuously. This study provides a further clarification of the specific composition and structure of the complex precipitates of arsenic sulfide, which will benefit the efficient stabilization of the arsenic sulfide sludge.

**Keywords:** sulfurization; precipitate-As(III); precipitate-As(V); elemental S; As<sub>2</sub>S<sub>3</sub>



**Citation:** Xu, H.; Wang, Y.; Yao, L.; Ke, Y.; Luo, Y.; Zhang, L.; Du, J.; Yu, L.; Cao, J.; Min, X. Treatment of Acidic Solutions Containing As(III) and As(V) by Sulfide Precipitation: Comparison of Precipitates and Sulfurization Process. *Metals* **2023**, *13*, 794. <https://doi.org/10.3390/met13040794>

Academic Editors: Jean François Blais and Petros E. Tsakiridis

Received: 10 January 2023

Revised: 10 February 2023

Accepted: 16 March 2023

Published: 18 April 2023



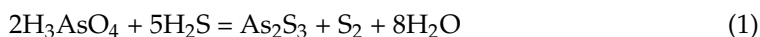
**Copyright:** © 2023 by the authors. Licensee MDPI, Basel, Switzerland. This article is an open access article distributed under the terms and conditions of the Creative Commons Attribution (CC BY) license (<https://creativecommons.org/licenses/by/4.0/>).

## 1. Introduction

Arsenic is a typical pollutant in the metallurgical process, distributing in flue gas, wastewater, slag, sludge, and residue with various degrees. During the smelting of non-ferrous metals-bearing concentrates, most of the arsenic is volatilized and oxidized to As<sub>2</sub>O<sub>3</sub> and As<sub>4</sub>O<sub>6</sub> and then emitted with flue gas. Prior to the sulfuric acid production, arsenic compounds in flue gas must be eliminated because the arsenic influences the quality of the produced sulfuric acid. Hence, spray washing with the diluted acid is performed to remove the dust and arsenic from the pre-cleaned gas. It is worth mentioning that a large quantity of arsenic-containing acidic wastewater is discharged when flue gas is spray washed with dilute acid [1–3]. To remove arsenic from wastewater, numerous methods, including precipitation, adsorption, coagulation, and membrane separation, have been developed [4–6]. While sorption, coagulation, and membrane separation are generally only used for removal of low levels of arsenic up to 30 μmol/L. Precipitation is suited for the removal of arsenic from acidic, arsenic-rich wastewaters: precipitation as calcium arsenate, ferric arsenate, or arsenic sulfide. Furthermore, recent studies have shown that calcium arsenate is of large volumes and less stable than expected. Additionally, the ferric

arsenate is not stable for long term storage because the reducing conditions can result in the reduction and mobilization of iron and arsenic. This technique requires the presence or addition of iron in/to the wastewater [7]. Among these methods, sulfide precipitation has been widely applied, due to its simple process and high efficiency, the potential for selective arsenic and heavy metal removal, and the production of small amounts of waste sludge.

Whether the sulfide precipitate of acidic wastewater containing As(V) was  $\text{As}_2\text{S}_5$  or  $\text{As}_2\text{S}_3$  and S was always controversial in 1826–1915. Berzelius (1826) proposed that hydrogen sulfide reacted with arsenic(V) acid would produce  $\text{As}_2\text{S}_5$  directly, while Rose (1859) considered the precipitate was composed of  $\text{As}_2\text{S}_3$  and elemental S [8]:



McCay (1887) proposed that arsenic(V) acid reacted with hydrogen sulfide to form  $\text{H}_3\text{AsO}_3\text{S}$  at first, and then  $\text{H}_3\text{AsO}_3\text{S}$  easily decomposed and produced arsenite and elemental S, due to its instability [8]. Usher and Travers (1905) proposed that there were significant differences in the precipitates obtained from arsenic(V) acid with varying concentrations of HCl. In the presence of 1.8% HCl, 91%  $\text{As}_2\text{S}_5$  was gathered. When the concentration of HCl increased to 7.9–14.34%, pure  $\text{As}_2\text{S}_5$  was obtained. When the concentration of HCl increased to 25.1%, 58%  $\text{As}_2\text{S}_5$  was produced [9,10]. Hattori obtained  $\text{As}_2\text{S}_3$  and  $\text{As}_2\text{S}_5$  with specific surface areas of  $17.6 \text{ m}^2/\text{g}$  and  $10.8 \text{ m}^2/\text{g}$  by hydrothermal sulfide precipitation [11].

In recent years, with the application of improved analytical methods and advanced characterization instruments, the mechanism of the sulfide precipitation of arsenic(III/V) acid has been further explored. Elizabeth et al. studied the reduction and precipitation of arsenate with sulfide and demonstrated that arsenite was not the direct product. Rather, the trimeric species ( $\text{H}_x\text{As}_3\text{S}_6^{x-3}$ ) developed, which could persist in the solution for several days [12]. Due to the formation and transformation of the intermediate species, which are the rate-controlling steps in the removal of As(V) from acidic wastewater, numerous studies have reported the promotion of UV light to improve the reduction rate and the removal efficiency [13–15]. For the sulfide precipitation of acidic wastewater containing As(III), it was concluded that As(III) reacted with  $\text{H}_2\text{S}$  immediately to precipitate as  $\text{As}_2\text{S}_3$  under excess S(-II). However, the formation of amorphous  $\text{As}_2\text{S}_3$  and  $\text{As}_4\text{S}_4$  in the process of adsorption and precipitation from acidic wastewater containing As(III) and As(V) by some sulfide minerals has been detected [16–20].

In summary, most of the studies focused on the As removal efficiency in solution, but there were few systematic studies on the characteristics of the precipitates. In particular, the morphology, valence, and characteristics of elemental S formed by reduction have not been mentioned. In fact, the sulfide precipitates, which were mainly composed of  $\text{As}_2\text{S}_3$ , have a long-term environmental risk, and their safety disposal is of great importance in non-ferrous industry [21]. Our recent work investigated the hydrothermal stabilization of two types of arsenic sulfide sludge (ASS) and demonstrated that the ASS containing elemental sulfur originally more easily achieved stabilization than the hydrothermal process of ASS without elemental sulfur originally [22]. To stabilize the hazardous solid waste (ASS), the specific composition and structure of the complex precipitates of arsenic sulfide are worth further clarification. In this study, the characteristics of sulfide precipitates from acidic wastewater containing As(III) and As(V) and the effects of temperature, the S(-II) to As(III)/(V) ratio (S/As), the volume fraction of  $\text{H}_2\text{SO}_4$  ( $\varphi_{\text{H}_2\text{SO}_4(\text{v})}$ ), and the concentration of  $\text{Cl}^-$  ( $c_{\text{Cl}^-}$ ) on sulfurization were investigated in detail.

## 2. Materials and Methods

### 2.1. Reagents and Materials

Sodium arsenite ( $\text{NaAsO}_2$ ), sodium arsenate ( $\text{Na}_3\text{AsO}_4 \cdot 12\text{H}_2\text{O}$ ), sodium sulfide ( $\text{Na}_2\text{S} \cdot 9\text{H}_2\text{O}$ ), sulfuric acid ( $\text{H}_2\text{SO}_4$ ), and sodium chloride (NaCl) used were analytical reagent (AR) grade and were purchased from Sinopharm Chemical Reagent Co., Ltd. (Shanghai, China). Deionized water was used in all experiments. Two stock solutions

of As(V) and As(III) were made by adding  $\text{H}_2\text{SO}_4$  and  $\text{NaAsO}_2/\text{Na}_3\text{AsO}_4 \cdot 12\text{H}_2\text{O}$  to the deionized water. The concentrations of As(III) and As(V) were both 0.05 mol/L and  $\varphi_{\text{H}_2\text{SO}_4(\text{v})}$  was 5%. The two kinds of stock solution of S(-II) with concentrations of 0.075 and 0.125 mol/L were prepared by dissolving  $\text{Na}_2\text{S} \cdot 9\text{H}_2\text{O}$ .

## 2.2. Experimental Procedure

The sulfide precipitation experiment was conducted in a 500 mL conical bottle containing a prepared acidic solution containing As(III)/As(V) with a thermostatic electromagnetic agitator (Aika, Germany), and dissolved sulfide was added for sulfide precipitation under the desired conditions (Figure 1). It is important to emphasize that all experiments were carried out under dark and airtight conditions.

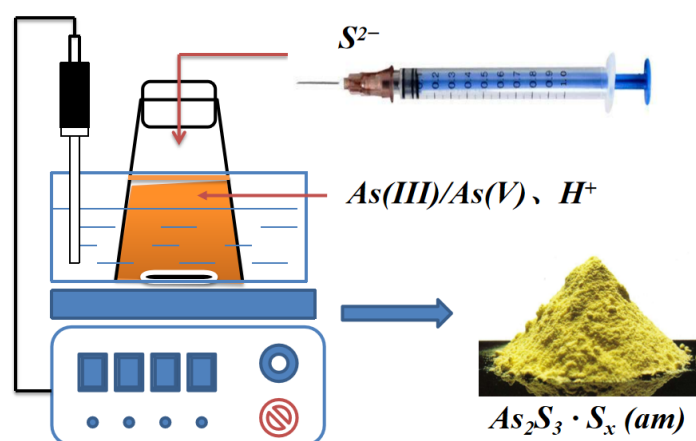


**Figure 1.** Experimental setup for the sulfide precipitation process.

For preparation of the sulfide precipitate of As(III), sulfide precipitation was carried out at 25 °C, with a S(-II)/As(III) ratio of 1.5 for 24 h, and the stirring rate was 400 r/min. For As(V), the experiment was conducted with the S(-II)/As(V) of 2.5, while the other conditions were kept at constants of 25 °C, 24 h, and 400 r/min.

To investigate the effects on the sulfide precipitation process of As(III), experiments were conducted at 0 °C, 30 °C, and 60 °C, the S(-II)/As(III) of 0.5, 1, 1.5, and 2.5, while the reaction time and stirring rate were kept at 24 h and 400 r/min. For As(V), the temperature of 0 °C and 30 °C, the S(-II)/As(V) of 1, 1.5, 2.5, and 3.75,  $\varphi_{\text{H}_2\text{SO}_4(\text{v})}$  of 0.5%, 1%, 2.5%, and 5%, the  $c_{\text{Cl}^-}$  of 0.01 mol/L, 0.1 mol/L, 0.25 mol/L, 0.5 mol/L, and 1 mol/L were investigated for 24 h and with 400 r/min constantly.

The precipitates obtained were separated by centrifugation, washed with deionized water at a liquid-solid ratio of 10:1 for 3 times, and then dried in a vacuum oven of 60 °C for subsequent analysis.

## 2.3. Analytical Methods

To determine quantitative elemental composition, the precipitates were dried at 60 °C in a vacuum oven (Lichen Bangxi Instrument Technology Co., Ltd., Shanghai, China). Then, they were ground and sieved to obtain samples with particle sizes of 100–200 mesh. Therewith, the samples were digested using a mixture of concentrated HCl and  $\text{HNO}_3$  (3:1, v/v). The solutions were filtrated with filter paper (1  $\mu\text{m}$  pore), and then element concentrations in filtrate were analyzed by inductively coupled plasma atomic emission spectrometer (ICP-AES, Agilent 5100, Agilent Technologies Co., Ltd., Shanghai, China).

The phases of the precipitates were analyzed by X-ray diffraction (XRD, Rigaku D/max 2500 VB + 18 kW, Rigaku Corporation, Tokyo, Japan) with a scanning speed of  $10^\circ \text{min}^{-1}$  from  $10^\circ$  to  $80^\circ$ . The microstructural observation and elemental composition were performed by scanning electron microscopy equipped with energy dispersive X-ray spectrometry (SEM-EDS, JSM-6300LV, JOEL Co., Ltd., Tokyo, Japan) and transmission

electron microscopy (TEM, JEM-2100F, JOEL Co., Ltd., Tokyo, Japan). The molecular structure was identified by Raman spectra (LABRAM-HR 800, Horiba Jobin-Yvon Ltd., Paris, France), recorded with a 513-nm-wavelength He-Ne laser and an acquisition time of 10 s and FTIR spectra (Nicolet IS50, Thermo Electron Co., Ltd., Atkinson, NH, USA), collected at  $4\text{ cm}^{-1}$  resolution. The surface composition was characterized by X-ray Photoelectron Spectroscopy (XPS, ESCALAB250Xi, Thermo Fisher Scientific, Waltham, MA, USA) with a Thermo Fisher Scientific K-Alpha (Thermo Fisher Scientific, Waltham, MA, USA) 1063 using Al-K $\alpha$  radiation.

### 3. Results and Discussion

#### 3.1. Characterization of Precipitates Sulfurized from As(III) and As(V)

##### 3.1.1. Appearance, Morphology, and Elemental Composition

As(III) reacted directly with S(-II) to form an orange–yellow precipitate and, once dissolved, sulfide was added into the acidic solution. For sulfide precipitation of acidic solution containing As(V), the precipitate was milky in the initial half hour and then gradually turned yellow. After 24 h, the arsenic sulfide precipitate was bright yellow, which was lighter than the precipitate-As(III) (Figure 2). Additionally, the removal efficiency of As(III) and As(V) could reach above 80% and 95%, respectively, which was slightly below the removal of 99% and 84% of As(III) and As(V) by reacting at a S:As molar ratio of 2.5 and 5 [7].

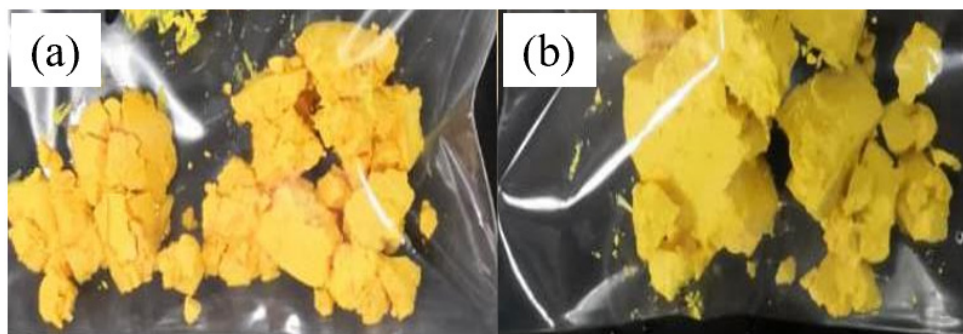


**Figure 2.** Picture of the precipitates: (a) precipitate-As(III); (b) precipitate-As(V).

The morphologies of the precipitate-As(III) and precipitate-As(V) are shown in Figure 3. It was obvious that the precipitate-As(III) was composed of large flocs aggregated by fine particles. The loose and porous flocs were irregular in shape, but the fine particles were uniformly distributed, and the main elements were arsenic and sulfur (Figure 3a,b). As shown in Table 1, the contents of As and S were 60.37% and 39.73%, with a S to As ratio of 1.54, which deviated slightly from the theoretical value of  $\text{As}_2\text{S}_3$ . Figure 3c shows that the precipitate-As(V) was composed of loose and porous flocs agglomerated by spherical particles with uneven size distribution. The microstructure of precipitate-As(V) was more complex than that of precipitate-As(III). The contents of arsenic and sulfur were 47.46% and 52.64% (Table 1), with the S to As ratio of 2.60, which differed from the theoretical value of  $\text{As}_2\text{S}_5$  or  $\text{As}_2\text{S}_3\text{-S}$  obtained by complete reduction and sulfide precipitation. The particles of precipitate-As(III) were finer in size and larger in specific surface area. This was consistent with the conclusion drawn by Hattori, i.e., that the specific surface areas of the precipitates formed by sulfide precipitation of As(III) and As(V) were  $17.6\text{ m}^2/\text{g}$  and  $10.8\text{ m}^2/\text{g}$ , respectively [11].

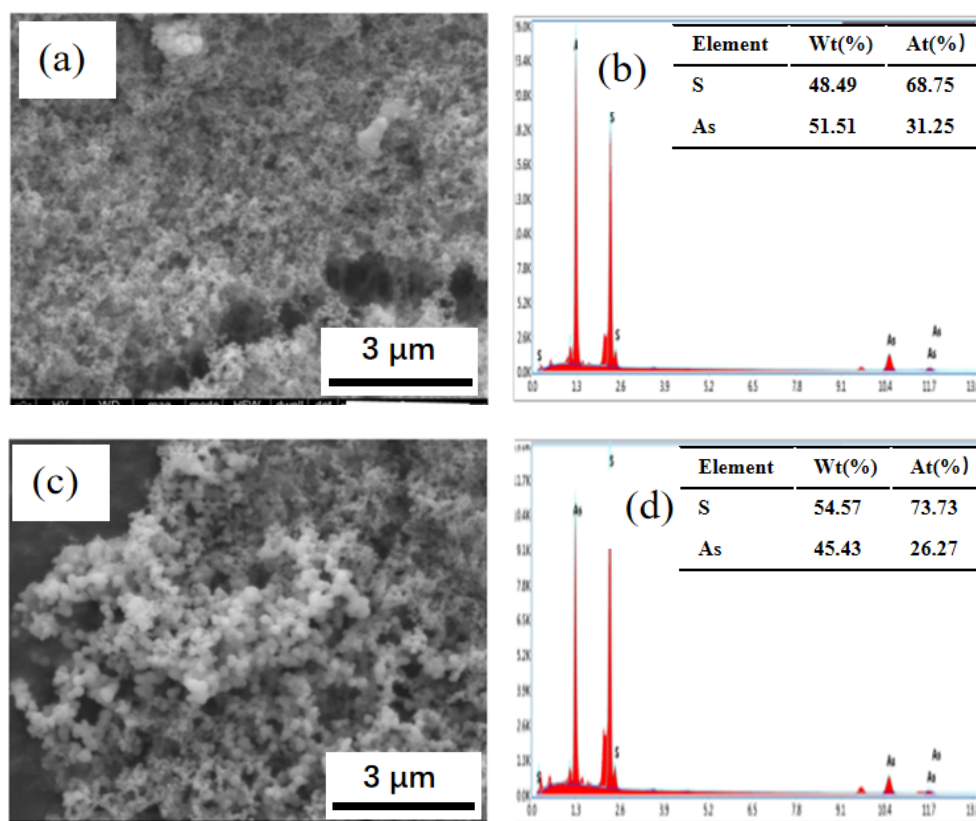


**Figure 3.** (a) SEM image of the precipitate-As(III); (b) EDS image of the precipitate-As(III); (c) SEM image of the precipitate-As(V); (d) EDS image of the precipitate-As(V).

**Table 1.** The main elemental composition of the precipitates.

Samples	Precipitate-As(III)		Precipitate-As(V)	
	As	S	As	S
Wt.%	60.37	39.73	47.46	52.64

As shown in Figure 4a, the precipitate-As(III) presented a network flocculent structure cross-linked by homogeneous nanoparticles. The particle size ranged 50–100 nm and expressed various microscopic morphologies. In addition, no diffraction spots of the crystal were observed, which confirmed that the precipitate-As(III) was amorphous.

The TEM images of precipitate-As(V) indicate that the precipitate expressed an adhesive structure cross-linked by particles of two sizes (Figure 4c). Many small spherical nanoparticles ranging 50–100 nm were attached around large particles ranging 200–500 nm. Few crystal diffraction points appeared that may be associated with crystal sulfur.

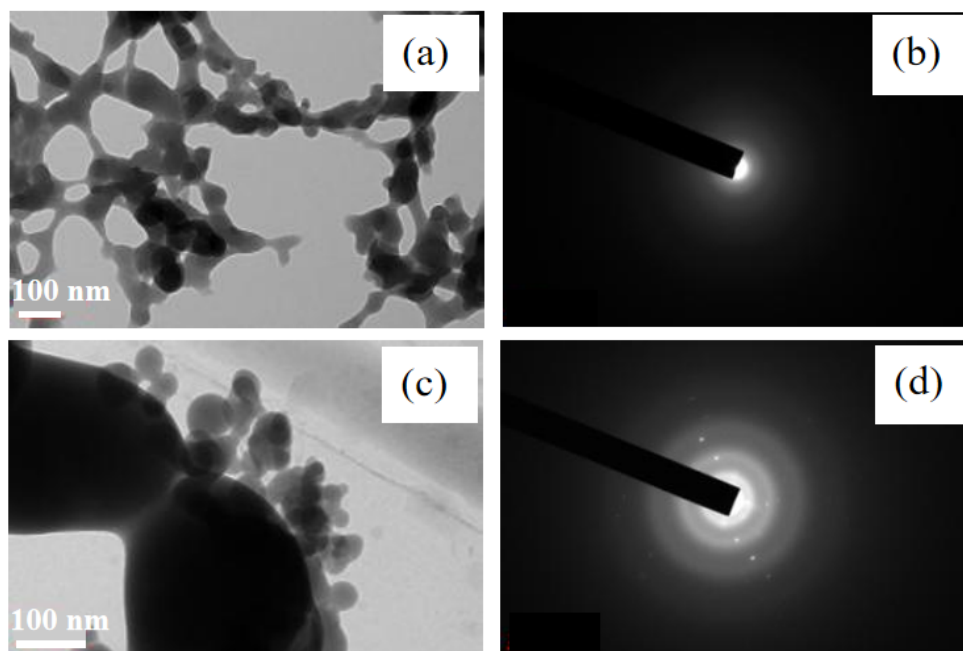


**Figure 4.** (a) TEM image of the precipitate-As(III); (b) SAED image of the precipitate-As(III); (c) TEM image of the precipitate-As(V); (d) SAED image of the precipitate-As(V).

### 3.1.2. Phase

The XRD pattern of the precipitates sulfurized from As(III) and As(V), shown in Figure 5, indicates that the diffraction peaks were both weak and wide, confirming that the precipitates were mainly amorphous. In addition, the three broad humps that appeared at  $2\theta$ , around  $18^\circ$ ,  $31^\circ$ , and  $57^\circ$ , were similar to the characteristic peaks of amorphous  $As_2S_3$ , while the characteristic peaks of elemental sulfur were detected in the XRD pattern of the precipitate-As(V). The results showed that precipitate-As(III) and precipitate-As(V) were mainly composed of amorphous  $As_2S_3$ , while the latter contained elemental S, which decomposed along with  $As_2S_3$  by  $H_xAs_3S_6^{x-3}$  first formed during the sulfurization of As(V). The characteristic peaks of amorphous  $As_2S_3$  were consistent with those synthesized by other researchers through similar methods [13–15].

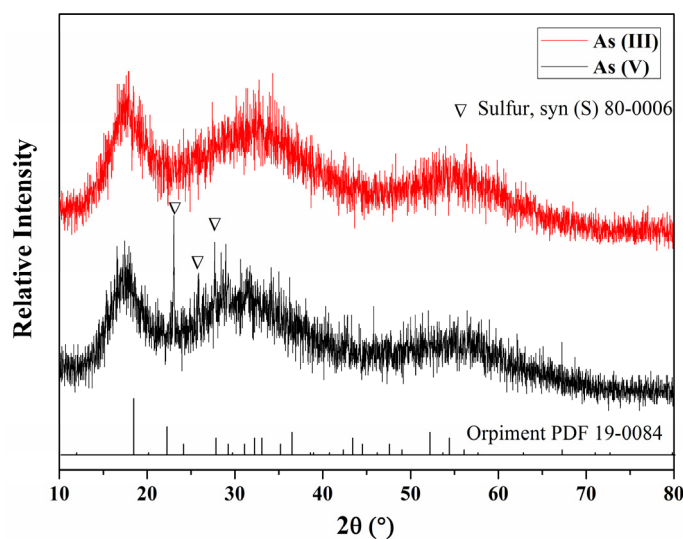


**Figure 5.** The XRD patterns of the precipitate-As(III) and the precipitate-As(V).

### 3.1.3. Molecular Structure

To clarify the molecular structure of the precipitate-As(III) and the precipitate-As(V), Raman and FTIR analyses were conducted. Figure 6 shows that there was one obvious characteristic peak located at approximately  $340\text{ cm}^{-1}$  related to the As-S bond in the  $\text{AsS}_{3/2}$  pyramidal structure in the precipitate-As(III) [23–25]. References for reported Raman spectra of different As-S compounds, namely the characteristic peak at  $340\text{ cm}^{-1}$ , correspond to orpiment, which is suited to the characteristic peaks in the precipitate-As(V) at around  $340\text{ cm}^{-1}$  [12]. In addition, three locations of  $153\text{ cm}^{-1}$ ,  $218\text{ cm}^{-1}$ , and  $473\text{ cm}^{-1}$  appeared, which should be related to the S-S bond of  $\text{S}_8$ . The Raman results were consistent with the SEM-EDS, TEM, and XRD observations.

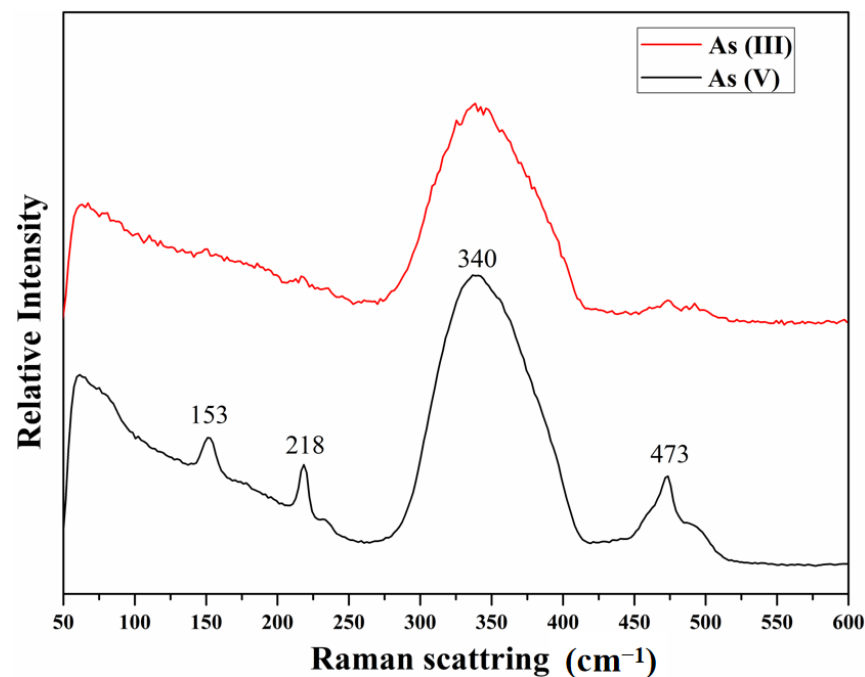


**Figure 6.** Raman spectra of the precipitate-As(III) and the precipitate-As(V).

The FTIR results of the precipitate-As(III) and the precipitate-As(V) are shown in Figure 7. Three peaks at approximately  $325\text{ cm}^{-1}$ ,  $355\text{ cm}^{-1}$ , and  $395\text{ cm}^{-1}$  were all observed in the precipitate-As(III), while the characteristic peaks in the precipitate-As(V) were mainly located at approximately  $325\text{ cm}^{-1}$  and  $355\text{ cm}^{-1}$ . The intensity of the peak at approximately  $325\text{ cm}^{-1}$  in the precipitate-As(III) was significantly higher than that in the precipitate-As(V), while the intensity of the peak at  $355\text{ cm}^{-1}$  was lower. It has been reported that the main characteristic peak in the structure of S-As glass is located at  $310\text{ cm}^{-1}$ , which corresponds to the As-S bond in the tapered structure of  $\text{AsS}_{3/2}$  [26,27]. In addition, there are two shoulder peaks at  $345\text{ cm}^{-1}$  and  $385\text{ cm}^{-1}$  in  $\text{As}_2\text{S}_3$  glass [28]. The phenomena above suggests that arsenic sulfide existed as  $\text{As}_2\text{S}_3$  in the precipitate-As(III) and the precipitate-As(V). Due to the difference in the structure of amorphous  $\text{As}_2\text{S}_3$  formed by precipitation in solution and  $\text{As}_2\text{S}_3$  glass, the three characteristic peaks ( $325\text{ cm}^{-1}$ ,  $355\text{ cm}^{-1}$ , and  $395\text{ cm}^{-1}$ ) in the precipitates from As(III) and As(V) all shifted approximately  $10\text{ cm}^{-1}$  with that of  $\text{As}_2\text{S}_3$  glass ( $310\text{ cm}^{-1}$ ,  $344\text{ cm}^{-1}$ , and  $385\text{ cm}^{-1}$ ).

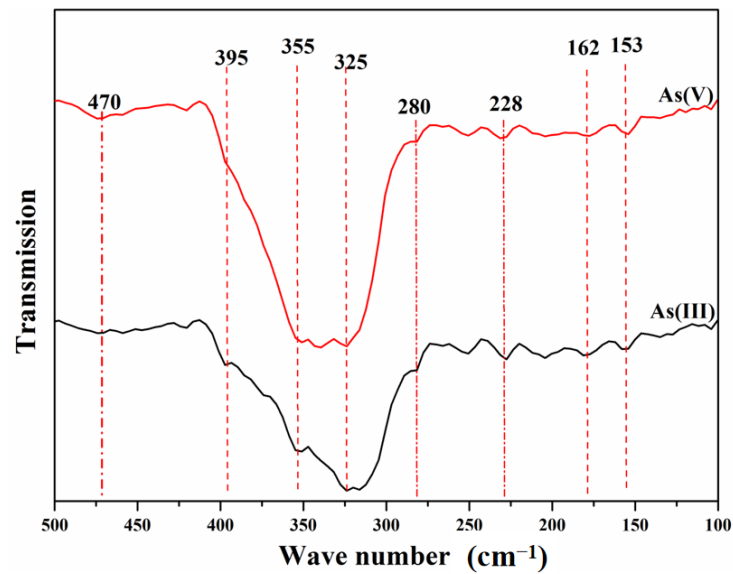


Figure 7. FTIR spectra of the precipitate-As(III) and the precipitate-As(V).

### 3.1.4. Surface Composition

Figure 8 and Table 2 show the As 3d and S 2p XPS spectra and the XPS Peak Parameters of the precipitate-As(III) and the precipitate-As(V). The As 3d spectra were modeled as doublets of  $3d_{3/2}$  and  $3d_{5/2}$ , separated by 0.69 eV. The area of the As  $3d_{3/2}$  peak was two-thirds the area of As  $3d_{5/2}$  peak. So, we will only discuss the details of As  $3d_{5/2}$  below because of their correlation.

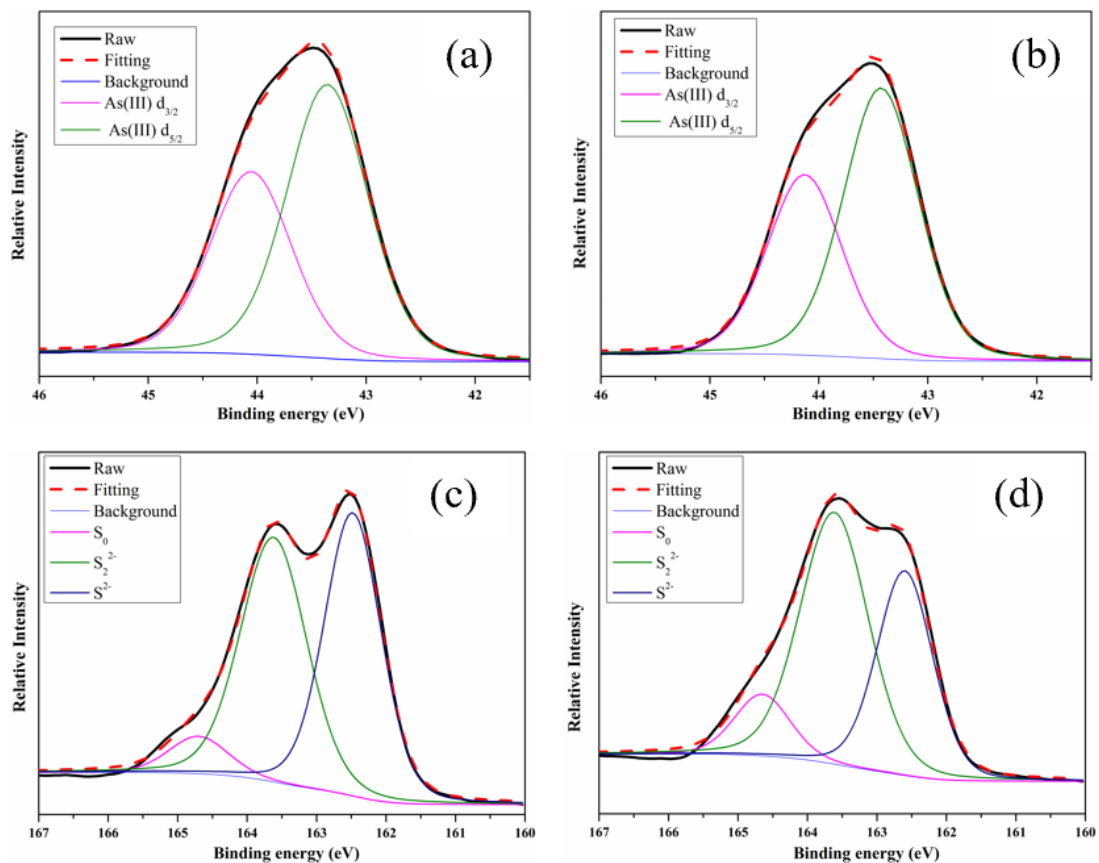


Figure 8. XPS spectra of (a) As 3d of precipitate-As(III); (b) As 3d of precipitate-As(V); (c) S 2p of precipitate-As(III); (d) S 2p of precipitate-As(V).

**Table 2.** Bending energy, FWHM, and peak positions from the XPS spectra of As 3d and S 2p.

Samples	XPS Peak Parameters	As 3d <sub>5/2</sub> As(III)	S <sup>0</sup>	S 2p S <sub>2</sub> <sup>2-</sup>	S <sup>2-</sup>
As(III)-S	BE (FWHM)	43.36 (0.883)	164.70 (1.00)	163.62 (1.12)	162.48 (0.96)
	Peak areas	100%	6.4%	46.9%	46.7%
As(V)-S	BE (FWHM)	43.43 (0.81)	164.65 (0.94)	163.61 (1.16)	162.60 (0.95)
	Peak areas	100%	10.7%	53.7%	35.6%

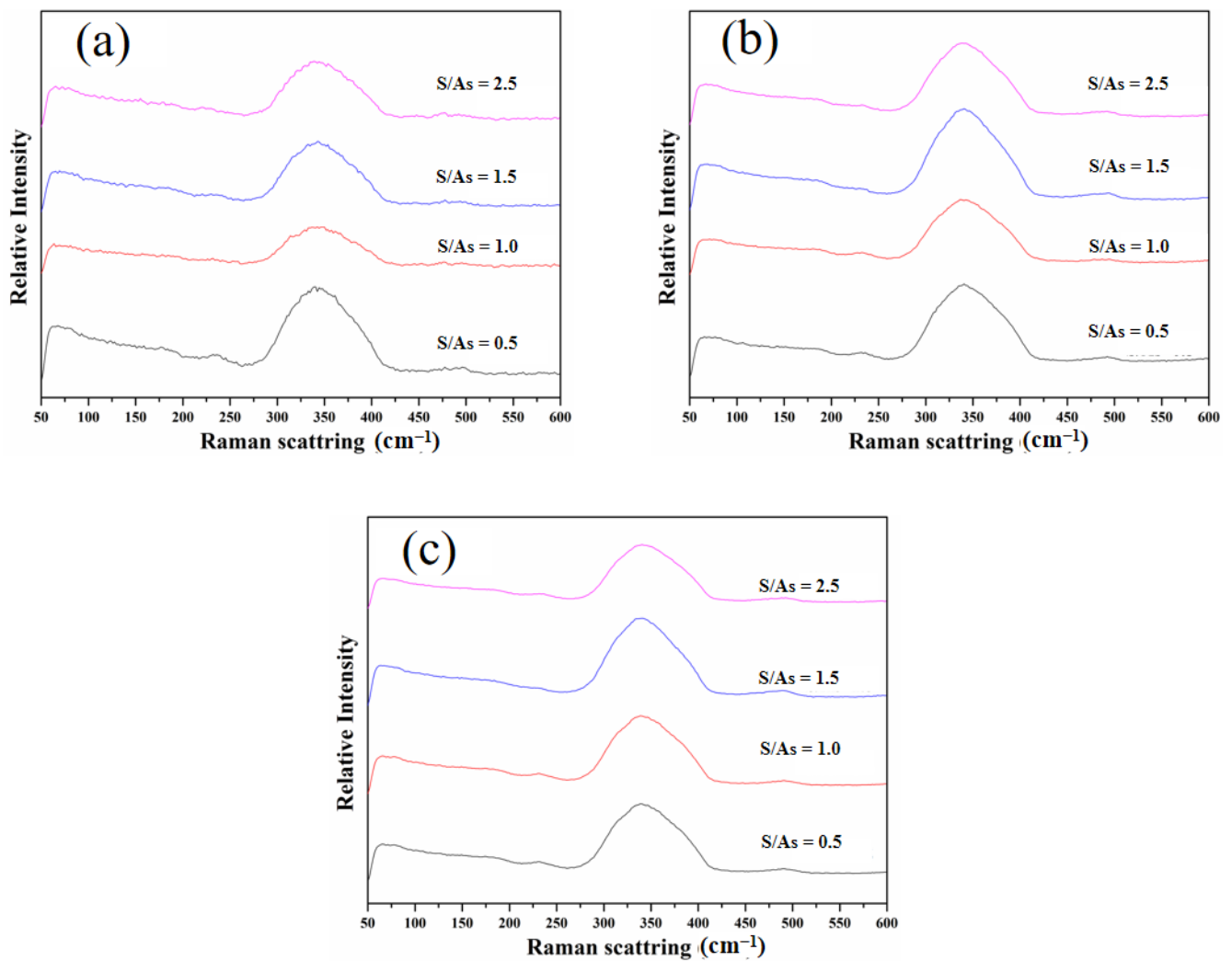
It has been reported that the peaks of As 3d<sub>5/2</sub> at 43.1 eV and 43.4 eV were attributed to As<sub>4</sub>S<sub>4</sub> and As<sub>2</sub>S<sub>3</sub> [17]. Additionally, the peaks of S 2p at 161.9 eV, 162.9 eV, and 164.1 eV were attributed to S<sup>2-</sup>, S<sub>2</sub><sup>2-</sup>, and polymeric sulfur (S<sup>0</sup>) [29,30]. Additionally, combined with the results shown in Table 1, the peaks of As 3d<sub>5/2</sub> in the precipitate-As(III) and the precipitate-As(V) at 43.4 eV were both attributed to As(III) in the As-S compound, and As(II) and As(V) did not appear, which is consistent with the results of Raman analysis, with only one characteristic peak of As<sub>2</sub>S<sub>3</sub> at 340 cm<sup>-1</sup>. The valences of As on the surface of the two precipitates were mainly As(III), indicating that As(V) first reacted with S<sup>2-</sup> to form H<sub>3</sub>AsO<sub>3</sub>S and then produced elemental S and As<sub>2</sub>S<sub>3</sub>. Because the As(III) and S(II) could be rapidly precipitated, the evidence that As(V) and As(III) were reduced to As(II) in solution to form As<sub>4</sub>S<sub>4</sub> has not been detected yet.

S 2p consisted of three prominent peaks at 162.7 eV, 163.6 eV, and 164.7 eV, corresponding to monosulfide (S<sup>2-</sup>), disulfide (S<sub>2</sub><sup>2-</sup>), and elemental sulfur (S<sup>0</sup>), respectively, showing that the speciation of S was significantly different, although the valence of As on the surface of the two precipitates was consistent. The contents of S<sup>0</sup> and S<sub>2</sub><sup>2-</sup> in precipitate-As(V) were higher than those of precipitate-As(III) by 4.3% and 6.8%, respectively, and S<sup>2-</sup> was lower by 11.1%. The difference in S was also directly analyzed by SEM-EDS and Raman. S (6.4%) was detected in the precipitate-As(III) by XPS, while no peak of elemental S was analyzed by Raman, which may have resulted from the strong energy radiation with XPS detection, causing decomposition of elemental sulfur. The differences between S<sup>0</sup> and S<sub>2</sub><sup>2-</sup> may directly lead to the differences in morphology and thermal property.

### 3.2. Sulfurization Process of As(III) and As(V)

#### 3.2.1. Effects on the Sulfurization Process of As(III)

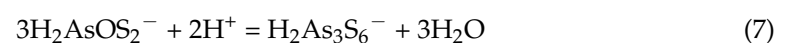
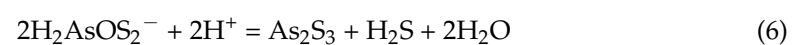
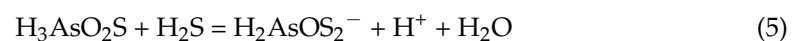
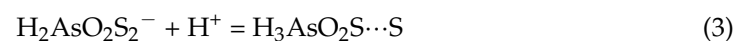
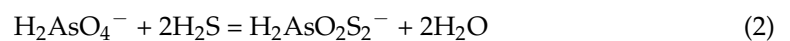
To investigate the influence of the temperature and the S(-II)/As(III) on the sulfurization process of acidic solutions containing As(III), experiments were conducted at temperatures of 0 °C, 30 °C, and 60 °C and the S(-II)/As(III) of 0.5, 1.0, 1.5, and 2.5 for 24 h. The Raman spectra of the precipitates-As(III), shown in Figure 9, indicate that the temperature and the S(-II)/As(III) were affected slightly within the whole studied range. Only the characteristic peak of As<sub>2</sub>S<sub>3</sub> at 340 cm<sup>-1</sup> was found, and no peak of S or other S-As compounds appeared. As As(III) reacted with S<sup>2-</sup> to form As<sub>2</sub>S<sub>3</sub> rapidly, the possibility of reducing As(III) to As(II) and producing elemental S was still very small, although the temperature and the S(-II)/As(III) were changed.



**Figure 9.** Raman spectra of the precipitates-As(III) for different S(-II)/As(III) at (a) 0 °C, (b) 30 °C, and (c) 60 °C.

### 3.2.2. Effects on the Sulfurization Process of As(V)

The Raman spectra of the precipitates-As(V) at different temperatures, S(-II)/As(V),  $\text{c}_{\text{Cl}^-}$ , and  $\varphi_{\text{H}_2\text{SO}_4(\text{v})}$  are shown in Figure 10. The precipitate-As(V) was slightly affected by S(-II)/As(V) at 0 °C, when the S(-II)/As(V) increased from 1.0 to 3.75, and the obvious peaks located at  $153\text{ cm}^{-1}$ ,  $218\text{ cm}^{-1}$ , and  $473\text{ cm}^{-1}$  related to elemental S, while the peaks at  $340\text{ cm}^{-1}$  of the As-S bond were weak. The result related to the following reactions [12]:



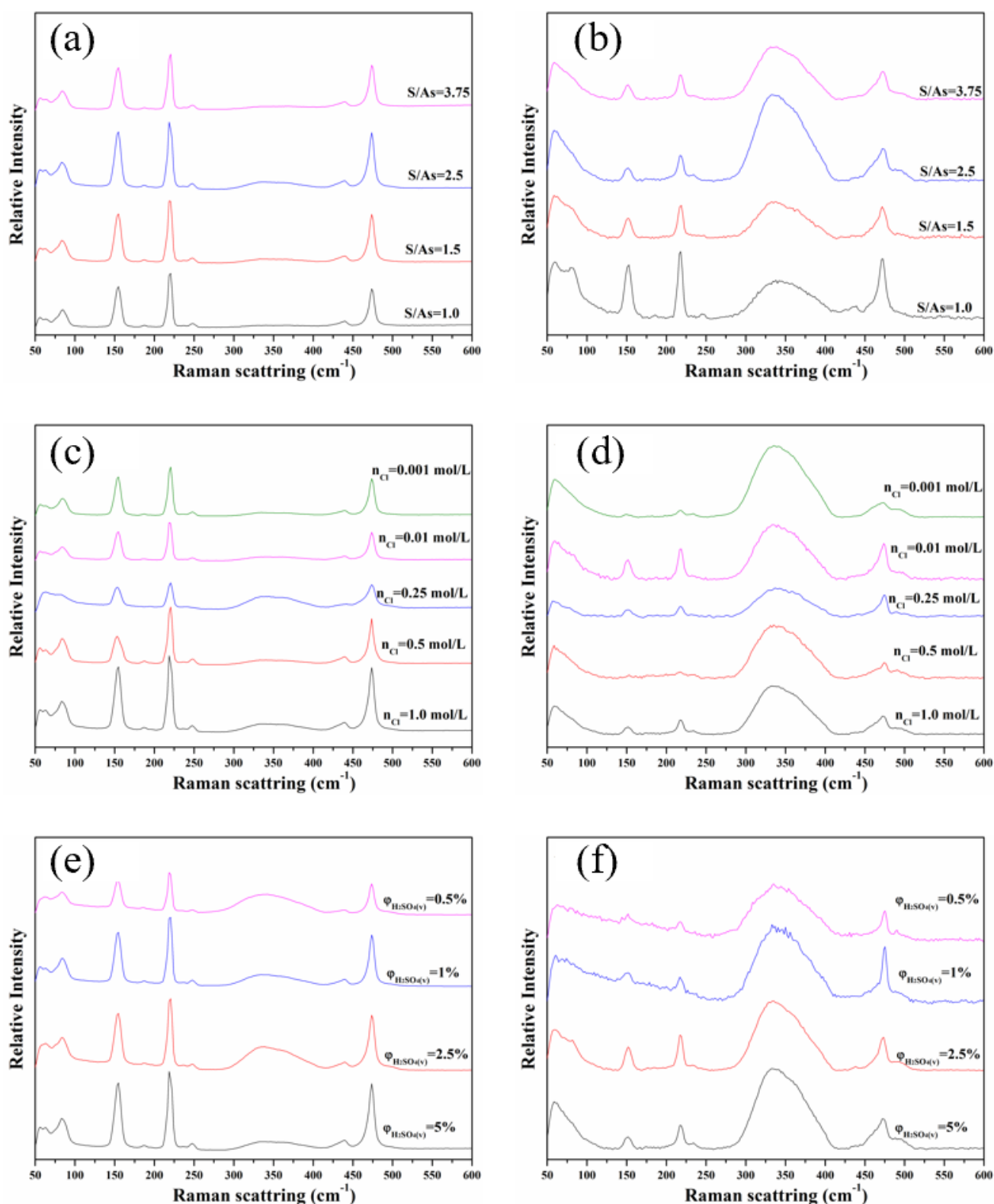


**Figure 10.** Raman spectra of the precipitates-As(V): (a) different S(-II)/As(V) at 0 °C; (b) different S(-II)/As(V) at 30 °C; (c) different  $c_{\text{Cl}^-}$  at 0 °C; (d) different  $c_{\text{Cl}^-}$  at 30 °C; (e) different  $\varphi_{\text{H}_2\text{SO}_4(\text{v})}$  at 0 °C; (f) different  $\varphi_{\text{H}_2\text{SO}_4(\text{v})}$  at 30 °C.

Reactions (2)~(4) occurred mainly when S(-II)/As(V) was low, and only a small amount of elemental S was produced due to the strong stability of  $\text{H}_2\text{AsOS}_2^-$  and  $\text{H}_x\text{As}_3\text{S}_6^{x-3}$  at low temperature. When the temperature raised to 30 °C, peaks at 340  $\text{cm}^{-1}$  obviously

appeared under different S(-II)/As(V), and the peak at  $340\text{ cm}^{-1}$  was further enhanced with the increase of S/As. Therefore, increasing temperature was not conducive to the stability of  $\text{H}_2\text{AsOS}_2^-$  and  $\text{H}_x\text{As}_3\text{S}_6^{x-3}$ , resulting in the decomposition to produce a large amount of  $\text{As}_2\text{S}_3$ . Herein, it is obvious that temperature and S(-II)/As(V) have the greatest influence on the sulfurization process of As(V), high temperature, and S/As promote the formation of  $\text{As}_2\text{S}_3$ .

The effect of  $c_{\text{Cl}^-}$  on the sulfurization of As(V) was more complex. There was only one wide peak at  $340\text{ cm}^{-1}$ , which was observed when the  $c_{\text{Cl}^-}$  was  $0.25\text{ mol/L}$  at  $0\text{ }^\circ\text{C}$ . When the temperature raised to  $30\text{ }^\circ\text{C}$ , the characteristic peak of elemental S almost disappeared with  $\text{Cl}^-$  of  $0.001\text{ mol/L}$  and  $0.5\text{ mol/L}$ , while the peak weakened at other concentrations. However, it has been reported that, in different concentrations of hydrochloric acid, the content of  $\text{As}_2\text{S}_3$  in As(V) sulfide precipitates varies greatly, but the exact mechanism is still unclear [9,10].

The  $\varphi_{\text{H}_2\text{SO}_4(\text{v})}$  also had a great influence on the precipitates-As(V). At  $0\text{ }^\circ\text{C}$ , the peaks at  $153\text{ cm}^{-1}$ ,  $218\text{ cm}^{-1}$ , and  $473\text{ cm}^{-1}$ , which related to the S-S bond of  $\text{S}_8$ , tended to weaken with acid concentration decreasing, and it shows a similar situation at  $30\text{ }^\circ\text{C}$ . A reasonable explanation could be obtained from reaction (7). The lower the concentration of  $\text{H}^+$  was more conducive for the decomposition of S, resulting in the constant weakening of the peaks at  $153\text{ cm}^{-1}$ ,  $218\text{ cm}^{-1}$ , and  $473\text{ cm}^{-1}$ . However, the peak at  $340\text{ cm}^{-1}$ , related to the As-S bond of  $\text{As}_2\text{S}_3$ , tended to strengthen with acid concentration decreasing at  $0\text{ }^\circ\text{C}$ , but decreased when acid concentration decreased at  $30\text{ }^\circ\text{C}$ , presenting a complicated effect on the production and dissolution of  $\text{As}_2\text{S}_3$ .

#### 4. Conclusions

The precipitate-As(III) mainly consisted of amorphous  $\text{As}_2\text{S}_3$  and was composed of large flocs aggregated by fine particles. The contents of As and S in the precipitate-As(III) were 60.37% and 39.73%, respectively. The As in precipitate-As(III) was mainly As(III), and S existed in the form of monosulfide ( $\text{S}^{2-}$ ), disulfide ( $\text{S}_2^{2-}$ ), and elemental sulfur ( $\text{S}^0$ ), with contents of 46.7%, 46.9%, and 6.4%, respectively. The precipitate-As(V) mainly consisted of amorphous  $\text{As}_2\text{S}_3$  and elemental S. It was composed of loose and porous flocs agglomerated by spherical particles with uneven size distribution. The contents of As and S in the precipitate-As(V) accounted for 47.46% and 52.64%, respectively. The As in precipitate-As(V) was mainly As(III), and S existed in the form of monosulfide ( $\text{S}^{2-}$ ), disulfide ( $\text{S}_2^{2-}$ ), and elemental sulfur ( $\text{S}^0$ ), with contents of 35.6%, 53.7%, and 10.7%, respectively.

Temperature and S(-II)/As(III) slightly affected the sulfurization process of As(III). For As(V), the temperature, S(-II)/As(V),  $c_{\text{Cl}^-}$ , and  $\varphi_{\text{H}_2\text{SO}_4(\text{v})}$  affected a lot. As the temperature increased, the content of  $\text{As}_2\text{S}_3$  in precipitate-As(V) increased significantly. When S(-II)/As(V) was low, the precipitate-As(V) consisted of elemental S and a small amount of  $\text{As}_2\text{S}_3$ . With the increase in S(-II)/As(V), the content of  $\text{As}_2\text{S}_3$  increased continuously. Additionally, the  $c_{\text{Cl}^-}$  also had a great influence on precipitate-As(V). For  $\varphi_{\text{H}_2\text{SO}_4(\text{v})}$ , the higher the concentration of  $\text{H}^+$ , the more  $\text{As}_2\text{S}_3$  produced.

**Author Contributions:** Conceptualization, Y.W. and L.Y. (Liwei Yao); methodology, H.X.; validation, Y.K. and X.M.; formal analysis, Y.L. and L.Z.; investigation, J.D., L.Y. (Lin Yu) and J.C.; resources, H.X. and Y.W.; data curation, H.X.; writing—original draft preparation, H.X.; writing—review and editing, H.X., Y.W. and L.Y. (Liwei Yao); visualization, Y.K.; supervision, X.M.; project administration, Y.W.; funding acquisition, X.M. All authors have read and agreed to the published version of the manuscript.

**Funding:** This research was supported by the National Key R&D Program of China (2018YFC1903301, 2018YFC1900301), National Science Fund for Distinguished Young Scholars (51825403), and National Natural Science Foundation of China (51634010, 51904354).

**Data Availability Statement:** Not applicable.

**Conflicts of Interest:** The authors declare no conflict of interest.

## References

1. Chai, L.; Yue, M.; Li, Q.; Zhang, G.; Zhang, M.; Wang, Q.; Liu, H.; Liu, Q. Enhanced stability of tooeleite by hydrothermal method for the fixation of arsenite. *Hydrometallurgy* **2018**, *175*, 93–101. [[CrossRef](#)]
2. Fei, J.; Ma, J.; Yang, J.; Liang, Y.; Ke, Y.; Yao, L.; Li, Y.; Liu, D.; Min, X. Effect of simulated acid rain on stability of arsenic calcium residue in residue field. *Environ. Geochem. Health* **2020**, *42*, 769–780. [[CrossRef](#)] [[PubMed](#)]
3. Ke, Y.; Shen, C.; Min, X.; Shi, M.; Chai, L. Separation of Cu and As in Cu-As-containing filter cakes by Cu<sup>2+</sup>-assisted acid leaching. *Hydrometallurgy* **2017**, *172*, 45–50. [[CrossRef](#)]
4. Min, X.; Peng, T.; Li, Y.; Ke, Y.; Liang, Y.; He, X. Stabilization of ferric arsenate sludge with mechanochemically prepared FeS<sub>2</sub>/Fe composites. *Trans. Nonferr. Metal. Soc.* **2019**, *29*, 1983–1992. [[CrossRef](#)]
5. Ke, P.; Liu, Z.; Li, L. Synthesis, characterization, and property test of crystalline polyferric sulfate adsorbent used in treatment of contaminated water with a high As(III) content. *Int. J. Miner. Mater.* **2018**, *25*, 1217–1225. [[CrossRef](#)]
6. Peng, B.; Song, T.; Wang, T.; Chai, L.; Yang, W.; Li, X.; Wang, H. Facile synthesis of Fe<sub>3</sub>O<sub>4</sub>@Cu(OH)<sub>2</sub> composites and their arsenic adsorption application. *Chem. Eng. J.* **2016**, *299*, 15–22. [[CrossRef](#)]
7. Ostermeyer, P.; Bonin, L.; Folens, K.; Verbruggen, F.; Garcia-Timmermans, C.; Verbeken, K.; Rabaey, K.; Hennebel, T. Effect of speciation and composition on the kinetics and precipitation of arsenic sulfide from industrial metallurgical wastewater. *J. Hazard. Mater.* **2020**, *409*, 124418. [[CrossRef](#)]
8. Brauner, B.; Tomiček, F. XII.—Action of hydrogen sulphide on arsenic acid. *J. Chem. Soc. Trans.* **1888**, *53*, 145–159. [[CrossRef](#)]
9. Foster, W. The action of hydrogen sulfide on arsenic acid. *J. Am. Chem. Soc.* **1916**, *38*, 52–57. [[CrossRef](#)]
10. Usher, F.; Travers, M. CXXXVII.—The interaction of sulphuretted hydrogen and arsenic pentoxide in presence of hydrochloric acid. *J. Chem. Soc. Trans.* **1905**, *87*, 1370–1373. [[CrossRef](#)]
11. Hattori, M.; Ogasawara, T. Heats of immersion of amorphous As<sub>2</sub>S<sub>3</sub>, As<sub>2</sub>S<sub>5</sub> and As<sub>2</sub>Se<sub>3</sub> in organic liquids. *Thermochim. Acta* **1983**, *63*, 51–58. [[CrossRef](#)]
12. Rochette, E.; Bostick, B.; Li, G.; Fendorf, S. Kinetics of arsenate reduction by dissolved sulfide. *Environ. Sci. Technol.* **2000**, *34*, 4714–4720. [[CrossRef](#)]
13. Kong, L.; Peng, X.; Hu, X. Mechanisms of UV-Light Promoted Removal of As(V) by Sulfide from Strongly Acidic Wastewater. *Environ. Sci. Technol.* **2017**, *51*, 12583–12591. [[CrossRef](#)] [[PubMed](#)]
14. Kong, L.; Peng, X.; Hu, X.; Chen, J.; Xia, Z. UV-Light-Induced Aggregation of Arsenic and Metal Sulfide Particles in Acidic Wastewater: The Role of Free Radicals. *Environ. Sci. Technol.* **2018**, *52*, 10719–10727. [[CrossRef](#)]
15. Peng, X.; Chen, J.; Kong, L.; Hu, X. Removal of arsenic from strongly acidic wastewater using phosphorus pentasulfide as precipitant: UV-light promoted sulfuration reaction and particle aggregation. *Environ. Sci. Technol.* **2018**, *52*, 4794–4801. [[CrossRef](#)]
16. Han, Y.; Gallegos, T.; Demond, A.; Hayes, K. FeS-coated sand for removal of arsenic(III) under anaerobic conditions in permeable reactive barriers. *Water Res.* **2011**, *45*, 593–604. [[CrossRef](#)]
17. Kim, E.; Batchelor, B. Macroscopic and X-ray Photoelectron Spectroscopic Investigation of Interactions of Arsenic with Synthesized Pyrite. *Environ. Sci. Technol.* **2009**, *43*, 2899–2904. [[CrossRef](#)]
18. Liu, R.; Yang, Z.; He, Z.; Wu, L.; Hu, C.; Wu, W.; Qu, J. Treatment of strongly acidic wastewater with high arsenic concentrations by ferrous sulfide (FeS): Inhibitive effects of S(0)-enriched surfaces. *Chem. Eng. J.* **2016**, *304*, 986–992. [[CrossRef](#)]
19. Renock, D.; Gallegos, T.; Utsunomiya, S.; Hayes, K.; Ewing, R.; Becker, U. Chemical and structural characterization of As immobilization by nanoparticles of mackinawite (FeS<sub>m</sub>). *Chem. Geol.* **2009**, *268*, 116–125. [[CrossRef](#)]
20. Rodriguez-Freire, L.; Sierra-Alvarez, R.; Root, R.; Chorover, J.; Field, J. Biomineralization of arsenate to arsenic sulfides is greatly enhanced at mildly acidic conditions. *Water Res.* **2014**, *66*, 242–253. [[CrossRef](#)]
21. Yao, L.; Min, X.; Ke, Y.; Wang, Y.; Liang, Y.; Yan, X.; Xu, H.; Fei, J.; Li, Y.; Liu, D.; et al. Release Behaviors of Arsenic and Heavy Metals from Arsenic Sulfide Sludge during Simulated Storage. *Minerals* **2019**, *9*, 130.
22. Xu, H.; Min, X.; Wang, Y.; Ke, Y.; Yao, L.; Liu, D.; Chai, Y. Stabilization of arsenic sulfide sludge by hydrothermal treatment. *Hydrometallurgy* **2020**, *191*, 105229. [[CrossRef](#)]
23. Arsova, D.; Boulmetis, Y.; Raptis, C.; Pamukchieva, V.; Skordeva, E. The boson peak in Raman spectra of As<sub>x</sub>S<sub>1-x</sub> glasses. *Semiconductors* **2005**, *39*, 960–962. [[CrossRef](#)]
24. Godelitsas, A.; Price, R.; Pichler, T.; Amend, J.; Gamaletsos, P.; Goettlicher, J. Amorphous As-sulfide precipitates from the shallow-water hydrothermal vents off Milos Island (Greece). *Mar. Chem.* **2015**, *177*, 687–696. [[CrossRef](#)]
25. Ward, A. Raman Spectroscopy of Sulfur, Sulfur-Selenium, and Sulfur-Arsenic Mixtures. *J. Phys. Chem.* **1968**, *72*, 4133–4139. [[CrossRef](#)]
26. Lucovsky, G.; Martin, R. A molecular model for the vibrational modes in chalcogenide glasses. *J. Non-Cryst. Solids* **1972**, *8–10*, 185–190. [[CrossRef](#)]
27. Zlatkin, L.; Markov, Y. On the nature of the optical vibrations in As<sub>2</sub>S<sub>3</sub> and As<sub>2</sub>Se<sub>3</sub> glasses. *Phys. Stat. Sol. (a)* **1971**, *4*, 391–396. [[CrossRef](#)]
28. Bertoluzza, A.; Fagnano, C.; Monti, P.; Semerano, G. Raman and infrared spectra of As<sub>2</sub>S<sub>x</sub> chalcogenide glasses with x ≤ 3. *J. Non-Cryst. Solids* **1978**, *29*, 49–60. [[CrossRef](#)]

29. Qiu, X.; Wen, J.; Huang, S.; Yang, H.; Liu, M.; Wu, B. New insights into the extraction of invisible gold in a low-grade high-sulfur Carlin-type gold concentrate by bio-pretreatment. *Int. J. Miner. Mater.* **2017**, *24*, 1104–1111. [[CrossRef](#)]
30. Yin, S.; Wang, L.; Wu, A.; Chen, X.; Yan, R. Research progress in enhanced bioleaching of copper sulfides under the intervention of microbial communities. *Int. J. Miner. Mater.* **2019**, *26*, 1337–1350. [[CrossRef](#)]

**Disclaimer/Publisher’s Note:** The statements, opinions and data contained in all publications are solely those of the individual author(s) and contributor(s) and not of MDPI and/or the editor(s). MDPI and/or the editor(s) disclaim responsibility for any injury to people or property resulting from any ideas, methods, instructions or products referred to in the content.